Effects of relativity and correlation on L-MM Auger spectra

Mau Hsiung Chen

Lawrence Livermore National Laboratory, P.O. Box 808, Livermore, California 94550

(Received 14 June 1984)

Relativistic computations of L_1-MM, L_2-MM, and L_3-MM Auger spectra have been carried out in the intermediate coupling with configuration interaction for a final two-hole state and j-j coupling for an initial state. Results for ten elements with $18 \leq Z \leq 92$ are listed and compared with experimental data. Good agreement with the scarce experimental data is attained. The effect of correlation is shown to shift some of the Auger energies by as much as ~ 15 eV. The effect of final-ionic-state configuration interaction is found to increase the L_3-M_1M_1 rate by a factor of ~ 2 for $Z \leq 45$. Intermediate coupling is necessary to analyze the L-MM Auger spectra for $30 \leq Z \leq 80$. As in the case of K-$M_1M_{4,5}$ transition calculated L_1-$M_3M_3(^3P_2)$ and L_3-$M_1M_{4,5}$ intensities as functions of Z are found to peak sharply in the neighborhood of $Z = 63$ due to the strong level-crossing interaction. This interaction is found to increase the L_1-$M_3M_3(^3P_2)$ intensity at $Z = 60$ by a factor of 50.

I. INTRODUCTION

The effects of relativity, spin-orbit mixing, and final-ionic-state configuration interaction have been found to be very important in analyzing the K-LL and K-MM Auger spectra.[1-3] For very light elements ($Z \leq 15$), the electrostatic interaction dominates and Russell-Saunders coupling applies. The effects of electron-electron Coulomb correlation are much more important than the effects of relativity for these light elements.[4-6] To predict relative intensities accurately, one should include not only final-ionic-state interaction but also final-state interchannel interaction.[7,8] For medium and heavy elements, relativistic effects become quite important, and the K Auger spectrum must be calculated relativistically in intermediate coupling with configuration interaction. The good agreement between theory and experiment for K Auger spectrum of medium and heavy elements[1-3] seems to indicate that the effects of final-state interchannel interaction become much less important for high-energy transitions.

Although there exist some nonrelativistic intermediate coupling calculations for L-MM Auger spectra for a few selected elements,[9,10] there is no systematic relativistic intermediate coupling calculations. Furthermore, the existing theoretical Auger energies are mostly obtained from the semi-empirical approach.[11,12] There are very few *ab initio* calculations of Auger energies. Here we report on theoretical L-MM Auger energies and transition rates from Dirac-Hartree-Slater (DHS) calculations in intermediate coupling with configuration interaction for ten elements with atomic number $18 \leq Z \leq 92$. The effects of correlation on Auger energies and the effect of strong level-crossing interaction on L-MM Auger intensities are also discussed.

II. THEORY

A. Relativistic intermediate coupling theory of Auger transitions

From perturbation theory, the Auger transition probability is

$$T_{if} = | \langle \psi_f | (H - E) | \psi_i \rangle |^2 , \qquad (1)$$

where ψ_i and ψ_f are the antisymmetrized many-electron wave functions for initial and final states, respectively. In the frozen-orbital approximation and in j-j coupling, Eq. (1) reduces to the two-hole-coupled Auger matrix element involving only active electrons,

$$T(\alpha JM\text{-}\alpha'J'M')$$
$$= | \langle j_1'j_2'J'M' | V_{12} | j_1j_2JM \rangle |^2 . \qquad (2)$$

Here $\langle j_1'j_2'J'M' |$ represents the initial antisymmetrized two-hole-coupled state, including the initial bound state j_1' ($n_1'\kappa_1'$) and the hole j_2' ($\epsilon\kappa_2'$) in the continuum that is filled by the emitted Auger electron. The final antisymmetrized two-hole-coupled state is denoted by $| j_1j_2JM \rangle$. The continuum wave function is normalized so as to represent one electron ejected per unit time. Atomic units are used unless indicated otherwise. Coupling between an outermost open shell and inner-shell vacancies is neglected in Eq. (1). This approximation is justified because the relatively weak coupling does not introduce any appreciable Auger-electron energy shift in transitions discussed in this paper. In the present relativistic calculations, the two-electron operator V_{12} is chosen according to the original Møller formula[13] which is, in the Lorentz gauge,

$$V_{12} = (1 - \vec{\alpha}_1 \cdot \vec{\alpha}_2)\exp(i\omega r_{12})/r_{12} , \qquad (3)$$

where the $\vec{\alpha}_i$ are Dirac matrices, and ω is the wave number of the exchanged virtual photon.

In the present calculations, the initial state is represented by a single j-j configuration. The final-ionic-state configuration interaction among all the possible final double-MM-hole states (i.e., $[M_iM_j]$; $i \leq j = 1$–5) is taken into account. For these calculations, j-j-coupled basis states are used. In j-j coupling, intermediate coupling can be treated as configuration interaction. Coulomb as well as Breit interactions are included in the energy matrix. The j-j configuration average energies were calculated from DHS wave functions[14] with the appropriate final-hole-

state configurations, including quantum-electrodynamic (QED) corrections. The energy splittings of the specific total J states of the two-hole-coupled configurations and off-diagonal matrix elements of the energy matrix were calculated by using a slightly modified general relativistic Auger program.[15] Eigenvalues and eigenfunctions were obtained by diagonalizing the energy matrix. The eigenfunctions with total angular momentum J can then be written as

$$\psi_\beta(J) = \sum_{\alpha=1}^{N} C_{\alpha\beta}(J)\phi_\alpha, \quad \beta=1,\ldots,N \qquad (4)$$

where $C_{\alpha\beta}(J)$ are the mixing coefficients and ϕ_α are the $j\text{-}j$-coupled basis states.

The Auger matrix element for the βth state is

$$M_\beta(J) = \sum_{\alpha=1}^{N} C_{\alpha\beta}(J)\langle \phi(j_1'j_2'JM) \mid V_{12} \mid \phi_\alpha(j_1j_2JM)\rangle . \qquad (5)$$

The total radiationless transition rate from $n_1'\kappa_1'$ to the βth eigenstate of the final two-hole-coupled states with eigenfunction $\psi_\beta(J)$ is

$$T_\beta(J) = \frac{2J+1}{2j_1'+1} \sum_{\kappa_2'} \mid M_\beta(J)\mid^2 . \qquad (6)$$

The relativistic Auger matrix elements in $j\text{-}j$ coupling were calculated from DHS wave functions that corresponding to the initial-hole-state configuration.[11] The detailed treatment of relativistic intermediate coupling with configuration interaction is described in Ref. 1.

B. Relativistic Auger transition energies

The earliest method to estimate Auger energies is based on a semiempirical approach. However, Auger transition energies are nowadays calculated by the ΔSCF method.[16] In terms of the relativistic model, a separated relativistic self-consistent-field (SCF) calculation is performed for initial single-hole and final double-hole states. The Auger energy is then determined by taking the energy difference. In our present DHS calculations, a first-order correction to the local potential approximation is made by computing the expectation value of the full Hamiltonian. This correction is essential in accurate calculations of transition energies.

The natural coupling scheme for the Dirac-Fock or Dirac-Hartree-Slater approach is $j\text{-}j$ coupling. Intermediate coupling is, however, more appropriate for the final two-hole states in most cases. For the relativistic SCF approach, intermediate coupling can be implemented either by diagonalizing the energy matrix of Coulomb and Breit interactions with respect to fixed $j\text{-}j$ coupled basis states[1] or by using the multiconfiguration Dirac-Fock approach in which the radial wave functions are optimized simul-

taneously with the diagonalization of the Hamiltonian matrix.[16] In our present calculations, fixed $j\text{-}j$-coupled basis states are employed. The QED corrections: vacuum polarization for all levels and self-energy for L levels are also included in the calculations.

The effect of electron-electron Coulomb correlation on Auger energies is largely ignored in most existing calculations. In principle, one should find the correlation contribution to the Auger energies by calculating the total correlation energies for initial and final states and taking the difference. This, however, is a very expensive proposition, and a more tractable procedure needs to be chosen. In first approximation, the correlation energies of the passive electrons from initial and final states can be assumed to cancel each other completely. We further assume that the correlation contribution to the binding energies of the final double-hole states can be estimated by summing the correlation contribution to the binding energies for the single-hole states. Hence, we only concern ourselves here with three important correlation contributions to the transition energy, namely, the ground-state correlation correction, the energy shift due to the Coster-Kronig or super-Coster-Kronig fluctuation of the hole states, and the final-ionic-state configuration interaction. In our present work, the first two corrections are equivalent to the corresponding corrections for the binding energies.

The ground-state correlation correction arises because of the broken pairs in the hole states. This correction can be evaluated from nonrelativistic theory as a sum of surviving pair energies after cancellation between ground and hole states,[17]

$$E_{gc}(a) = \frac{1}{2(2l_a+1)} \sum_b E_{vv'}^0(a,b) + \frac{1}{2l_a+1} E_{vv'}^0(a,a) , \qquad (7)$$

where $E_{vv'}^0(a,b)$ is the total pair energy between two closed shells,

$$E_{vv'}^0(a,b) = \sum_{L,S}(2S+1)(2L+1)\epsilon(n_a 1_a, n_b 1_b; SL) , \qquad (8)$$

with $\epsilon(n_a 1_a, n_b 1_b; SL)$ being the symmetry-adapted pair energy.

Another important correlation contribution to the binding energy is caused by dynamic relaxation processes in which the core hole fluctuates to intermediate levels of the Coster-Kronig or super-Coster-Kronig type, in addition to creating electron-hole pair excitations.[17,18] If the transitions are energetically impossible, these effects always reduce the binding energies: they can be estimated by finite configuration-interaction or multiconfiguration Hartree-Fock (MCHF) methods.

When the hole state is embedded in the (super-) Coster-Kronig continua, we can use Fano's[19] approach of configuration interaction with the continuum to calculate the energy shift. Neglecting the effect of channel coupling and using the fixed-energy approximation, the energy shift due to the interaction with the continua can be obtained by calculating the principal-value integrals,[20]

TABLE I. Theoretical L_3-MM Auger energies (in eV).

Final state	$_{18}$Ar	$_{30}$Zn	$_{36}$Kr	$_{45}$Rh	$_{54}$Xe	$_{60}$Nd	$_{67}$Ho	$_{70}$Yb	$_{80}$Hg	$_{92}$U
$M_1M_1(^1S_0)$	164.7	704.2	1055.4	1695.4	2430.3	2989.1	3738.1	4072.8	5047.8	5920.5
$M_1M_2(^1P_1)$	181.9	749.2	1121.7	1800.0	2579.3	3168.0	3955.7	4308.3	5347.5	6309.7
$M_1M_2(^3P_0)$	189.6	764.3	1139.1	1818.8	2597.1	3186.7	3977.4	4328.0	5369.4	6334.6
$M_1M_3(^3P_1)$	189.6	765.5	1142.6	1832.8	2640.8	3269.2	4127.8	4521.7	5766.3	7175.8
$M_1M_3(^3P_2)$	189.7	767.4	1147.3	1844.5	2660.2	3293.9	4157.4	4553.4	5805.0	7222.9
$M_2M_2(^1S_0)$	203.2	803.8	1197.9	1909.9	2725.2	3340.1	4161.9	4530.8	5629.2	6674.8
$M_2M_3(^1D_2)$	204.9	806.2	1204.7	1933.3	2786.0	3444.4	4341.5	4753.4	6061.6	7561.1
$M_2M_3(^3P_1)$	206.8	813.3	1212.8	1943.4	2797.3	3457.0	4493.9	4767.5	6077.5	7579.2
$M_3M_3(^3P_0)$	206.8	813.2	1214.9	1958.2	2845.3	3546.2	4516.6	4790.5	6486.7	8434.3
$M_3M_3(^3P_2)$	207.0	815.5	1219.3	1965.5	2853.7	3551.6	4544.4	4994.6	6510.7	8462.0
$M_1M_4(^1D_2)$		844.0	1261.9	2018.7	2899.0	3578.3	4484.2	4905.6	6241.5	7767.2
$M_1M_4(^3D_1)$		846.1	1265.3	2202.2	2902.2	3577.3	4355.2	4914.2	6249.3	7775.2
$M_1M_5(^3D_2)$		846.3	1265.9	2025.5	2911.7	3598.8	4520.0	4950.6	6329.0	7938.9
$M_1M_5(^3D_3)$		846.5	1266.6	2027.7	2915.1	3602.2	4534.7	4962.7	6341.4	7954.3
$M_2M_5(^1F_3)$		886.8	1325.7	2121.0	3050.0	3764.4	4733.3	5178.3	6617.8	8315.7
$M_2M_4(^1P_1)$		889.4	1327.8	2117.6	3036.5	3736.8	4688.0	5124.4	6517.7	8125.5
$M_2M_4(^3D_2)$		894.9	1335.6	2131.5	3056.5	3761.7	4716.1	5154.3	6553.8	8170.3
$M_3M_4(^3D_1)$		895.5	1338.5	2146.3	3103.5	3850.6	4878.3	5358.2	6963.9	9027.2
$M_2M_5(^3P_2)$		897.2	1340.1	2135.3	3058.4	3773.0	4741.2	5186.1	6625.6	8323.8
$M_3M_4(^3D_3)$		896.4	1340.5	2149.1	3104.4	3851.5	4878.5	5358.3	6964.0	9027.4
$M_3M_4(^3P_0)$		897.9	1342.5	2151.5	3107.5	3853.6	4880.8	5360.7	6966.1	9029.0
$M_3M_5(^3P_1)$		897.8	1342.5	2152.2	3112.1	3866.8	4907.6	5394.1	7039.7	9185.2
$M_3M_4(^3F_2)$		900.5	1344.0	2153.2	3110.5	3858.1	4886.4	5366.8	6974.0	9039.3
$M_3M_5(^3F_3)$		902.4	1348.0	2158.8	3119.4	3875.4	4917.0	5404.0	7051.2	9199.1
$M_3M_5(^3F_4)$		903.8	1351.4	2167.6	3133.7	3894.3	4939.5	5428.0	7080.6	9234.6
$M_3M_5(^1D_2)$		902.6	1349.4	2163.6	3128.1	3886.9	4930.8	5418.8	7069.2	9220.8
$M_4M_4(^1S_0)$		974.5	1456.3	2323.3	3343.8	4131.2	5211.4	5715.3	7403.6	9574.0
$M_4M_5(^1G_4)$		978.8	1463.7	2336.8	3365.6	4166.3	5263.6	5776.0	7510.5	9771.3
$M_5M_5(^3P_0)$		979.8	1465.0	2339.3	3372.6	4181.5	5291.9	5810.6	7584.1	9925.7
$M_4M_4(^3P_2)$		979.9	1465.1	2336.6	3359.7	4149.8	5232.3	5737.4	7429.8	9605.6
$M_4M_5(^3P_1)$		979.8	1465.1	2338.4	3367.5	4167.5	5264.4	5776.6	7510.2	9769.6
$M_4M_5(^1D_2)$		980.6	1466.6	2341.3	3370.7	4171.4	5268.8	5781.3	7516.0	9776.9
$M_5M_5(^3F_2)$		982.3	1468.9	2345.8	3382.2	4194.5	5307.6	5827.6	7605.4	9952.3
$M_4M_5(^3F_3)$		982.5	1469.4	2345.2	3376.1	4178.1	5276.7	5789.7	7526.3	9789.4
$M_5M_5(^3F_4)$		982.8	1470.4	2350.0	3387.7	4201.2	5315.2	5835.7	7615.1	9964.1

$$\Delta E = \sum_{\lambda=1}^{N} P \int \frac{\left| \left\langle \psi_{\lambda\epsilon} \left| \sum_{i<j} r_{ij}^{-1} \right| \Phi \right\rangle \right|^2}{E_\phi - E_\lambda - \epsilon} \, d\epsilon \, . \qquad (9)$$

Here E_ϕ and E_λ are the threshold energies of the single-hole state and doubly ionized Auger continuum, respectively. The Auger matrix element $\langle \psi_{\lambda\epsilon} | \sum_{i<j} r_{ij}^{-1} | \Phi \rangle$ for channel λ is evaluated with the aid of a general relativistic program.[15] In our present work, the level shift ΔE is approximately energy independent.

III. RESULTS AND DISCUSSION

The calculated L_3-MM Auger energies are listed in Table I. The contributions from the effects of relaxation, Breit interaction, QED, and limited final-ionic-state configuration interaction are included in the calculations. However, the ground-state correlation and energy shift due to the interaction with the Coster-Kronig or Super-Coster-Kronig continua are not taken into account because these corrections are only considered for binding energies.

The QED corrections including self-energy and vacuum polarization on L-shell binding energies for heavy elements are quite significant. The L_1, L_2, and L_3 binding energies for $_{92}$U are reduced by ~ 39, 6, and 7 eV respectively.[14] The more detailed information on the QED

TABLE II. Level-energy shift (in eV) produced by configuration interaction with (super-) Coster-Kronig continua.

Atomic number Z	$2s$[a]	Level $3s$	$3p$
18	-2.2	-6.3	
30	-3.3	-4.5	-3.2
36	-5.0	-4.5	-4.7
45	-3.7		
54	-5.0	-3.5	-2.7
70		-7.9	-3.0
80	-4.2	-8.4	-4.7
92	-1.7	-6.9	-5.8

[a]From Ref. 20.

TABLE III. Theoretical and experimental Auger energies (in eV) for argon and gas-phase zinc.

| Element | Transition | Auger energy | | |
		DHS-ICCI	DHS-CORR	Expt.
$_{18}$Ar	L_3-M_1M_1	164.7	176.8	177.79[a]
	L_3-$M_{23}M_{23}(^1S_0)$	203.2	201.7	201.10[b]
	L_3-$M_{23}M_{23}(^1D_2)$	204.9	203.4	203.48[b]
	L_3-$M_{23}M_{23}(^3P)$	206.9	205.4	205.21[b]
$_{30}$Zn	L_3-$M_{2,3}M_{4,5}(^1F_3)$	886.8	886.7	886.7[c]
	L_3-$M_{4,5}M_{4,5}(^1G_4)$	978.8	973.8	973.3[c]

[a]From Ref. 10.
[b]From Ref. 23.
[c]From Ref. 22.

corrections can be found in Ref. 14.

The ground-state correlation effect is the dominant correlation contribution to the binding energy for an outermost shell, and for inner shells with orbital angular momentum $l = n - 1$, where n is the principal quantum number (e.g., $2p$ and $3d$ in our present calculations). This effect always increases the binding energy since all pair energies are negative and there are more pairs in the ground state than in the hole state. The ground-state correlation contributions to the binding energies were estimated to be ~ 1 eV for $2s$ and $3s$ levels and ~ 1.5 eV for $2p$ and $3p$ levels,[17] and ~ 3.3 eV for $3d$ level of $_{30}$Zn.[21]

The energy shifts of the single-hole states due to the interaction with the (super-) Coster-Kronig continua were calculated from Eq. (9) using DHS wave functions. The results for $2s$, $3s$, and $3p$ levels are listed in Table II. These effects are important for hole states that can decay by Coster-Kronig or super-Coster-Kronig transitions (e.g., $2s$, $3s$, and $3p$). However, they are quite negligible for $2p$ and $3d$ hole states.[20] In our present calculations, these energy shifts reduce the binding energies by 2—8 eV.

The correlation effect on the final two-hole state of an Auger transition is approximated by the sum of the contributions from individual hole states. The net effect of these correlation corrections on Auger transition energies depends on specific transition. The effects from three different levels could almost cancel completely (e.g., L_3-$M_{2,3}M_{4,5}$ of $_{30}$Zn). They can also add up and yield a large correction (e.g., 12 eV for L_3-M_1M_1 of $_{18}$Ar). Including these correlation corrections (DHS-CORR) leads to improved agreement between theoretical Auger energies and experimental results from gas-phase measurements[10,22,23] (Table III).

The calculated relativistic L-MM Auger transition rates in intermediate coupling with configuration interaction (DHS-ICCI) are listed in Tables IV—VI. The intensity ratios from Dirac-Hartree-Slater and Hartree-Slater calculations and experiment[24—32] are compared in Figs. 1—5. The effect of relativity on the individual Auger rates has been thoroughly studied. In our present calculations, the relativistic effect on some of the relative intensities [e.g., $I(L_3 - M_3M_5)/I(L_3 - M_2M_3)$ and $I(L_3 - M_3M_3)/I(L_3 - M_2M_3)$] is quite significant ($\sim 15$ —25%). In Fig. 1, the relative intensity $I(L_3 - M_1M_3(^3P_1))/I(L_3 - M_1M_3(^3P_2))$ as a function of

atomic number Z from Hartree-Slater in mixed coupling (i.e., j-j for the initial state and LS for the final state), Dirac-Hartree-Slater in j-j coupling, and Dirac-Hartree-Slater in intermediate coupling are compared with experiment.[24] The transition from LS coupling for low-Z atoms ($Z \leq 20$) to intermediate coupling for medium and medium-heavy ($20 \leq Z \leq 75$) and from intermediate coupling to j-j coupling for heavy elements ($Z \geq 75$) are clearly demonstrated. As in the cases of K-LL and K-MM Auger spectra, the effects of configuration interaction among $M_1M_1(J=0)$, $M_2M_2(J=0)$, and $M_3M_3(J=0)$ states are very important. These correlation effects in-
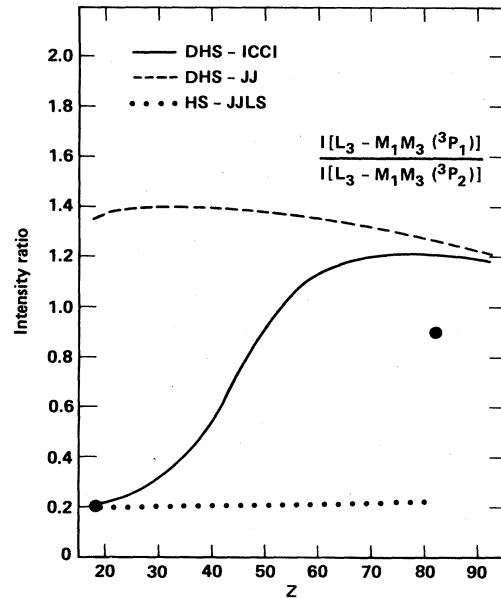
FIG. 1. Ratio of calculated L_3-$M_1M_3(^3P_1)$ Auger rate to L_3-$M_1M_3(^3P_2)$ Auger rate, as a function of atomic number. The solid curve represents Dirac-Hartree-Slater results in intermediate coupling with configuration interaction, the dashed curve indicates Dirac-Hartree-Slater results in j-j coupling, and the dotted curve represents the nonrelativistic Hartree-Slater results in mixed coupling scheme, all from the present work. The experimental results are from Ref. 24.

TABLE IV. Theoretical relativistic L_1-MM Auger transition rates [in milliatomic units (1×10^{-3} a.u. $=0.027\,21$ eV$/\hbar=4.134\times10^{13}$ s^{-1})], in intermediate coupling with configuration interaction. [Numbers enclosed in parentheses signify powers of 10; e.g., $8.41(-1)=8.41\times10^{-1}$.]

Final state	$_{18}$Ar	$_{30}$Zn	$_{36}$Kr	$_{45}$Rh	$_{54}$Xe	$_{60}$Nd	$_{67}$Ho	$_{70}$Yb	$_{80}$Hg	$_{92}$U
$M_1M_1(^1S_0)$	8.41(−1)	1.03	1.21	1.48	1.74	1.92	2.15	2.25	2.65	3.29
$M_1M_2(^1P_1)$	1.67	2.27	2.72	3.15	3.29	3.40	3.61	3.73	4.24	5.19
$M_1M_2(^3P_0)$	2.15(−1)	3.40(−1)	4.28(−1)	5.59(−1)	6.99(−1)	7.99(−1)	9.34(−1)	1.00	1.27	1.76
$M_1M_3(^3P_1)$	6.40(−1)	1.00	1.29	1.86	2.62	3.05	3.48	3.64	4.15	4.78
$M_1M_3(^3P_2)$	1.06	1.62	2.00	2.53	3.02	3.31	3.64	3.79	4.24	4.72
$M_2M_2(^1S_0)$	2.2(−2)	1.2(−2)	8.0(−3)	4.05(−3)	2.23(−3)	1.21(−3)	6.43(−4)	4.57(−4)	4.29(−5)	1.50(−4)
$M_2M_3(^1D_2)$	1.0(−2)	7.06(−1)	8.60(−1)	9.66(−1)	8.57(−1)	8.55(−1)	7.58(−1)	7.23(−1)	6.35(−1)	6.39(−1)
$M_2M_3(^3P_1)$	6.0(−6)	8.0(−5)	2.0(−4)	6.8(−4)	1.77(−3)	2.83(−3)	4.89(−3)	6.08(−3)	1.20(−2)	2.57(−2)
$M_2M_3(^3P_0)$	1.0(−4)	4.0(−3)	1.0(−2)	2.42(−2)	4.82(−2)	6.82(−2)	1.01(−1)	1.17(−1)	1.83(−1)	2.77(−1)
$M_3M_3(^3P_2)$	2.0(−6)	2.0(−2)	8.1(−2)	2.78(−1)	7.38(−1)	2.54	2.36	8.95(−1)	7.16(−2)	1.36(−2)
$M_3M_3(^3P_0)$	6.0(−6)	2.87	4.55	5.57	5.27	3.01	6.08	6.07	5.67	5.23
$M_1M_4(^1D_2)$		2.69(−1)	4.10(−1)	5.70(−1)	7.23(−1)	8.19(−1)	9.42(−1)	1.00	1.22	1.56
$M_1M_4(^3D_1)$		4.40(−1)	7.32(−1)	1.75	3.26	4.42	2.19	3.88	5.46	5.83
$M_1M_5(^3D_2)$		5.83(−1)	8.61(−1)	1.12	1.31	1.38	1.46	1.49	1.57	1.65
$M_1M_5(^3D_3)$		1.46	2.34	2.93	2.93	2.89	2.87	2.90	3.01	3.26
$M_2M_5(^1F_3)$		1.33(−1)	1.88(−1)	2.24(−1)	2.54(−1)	2.88(−1)	3.28(−1)	3.48(−1)	4.23(−1)	5.35(−1)
$M_2M_4(^1P_1)$		2.0(−3)	5.0(−3)	6.38(−3)	2.17(−3)	2.55(−3)	3.33(−3)	3.85(−3)	6.65(−3)	1.22(−2)
$M_2M_4(^3D_2)$		6.0(−3)	2.7(−2)	7.64(−2)	8.14(−2)	6.44(−2)	5.89(−2)	5.92(−2)	6.32(−2)	7.47(−2)
$M_3M_4(^3D_1)$		5.0(−3)	5.0(−3)	3.15(−3)	8.64(−3)	8.83(−3)	1.01(−2)	1.08(−2)	1.39(−2)	2.01(−2)
$M_2M_5(^3P_2)$		8.0(−3)	6.1(−2)	3.61(−1)	8.91(−1)	9.43(−1)	9.44(−1)	9.21(−1)	7.41(−1)	5.55(−1)
$M_3M_4(^3D_3)$		2.0(−3)	3.0(−3)	5.86(−3)	1.0(−2)	1.30(−2)	1.86(−2)	2.16(−2)	3.51(−2)	6.03(−2)
$M_3M_4(^3P_0)$		4.0(−3)	7.0(−3)	1.50(−2)	4.12(−2)	6.28(−2)	6.03(−2)	5.49(−2)	3.32(−2)	3.03(−2)
$M_3M_5(^3P_1)$		5.0(−3)	7.0(−3)	1.06(−2)	1.46(−2)	1.88(−2)	2.73(−2)	3.24(−2)	5.79(−2)	1.14(−1)
$M_3M_4(^3F_2)$		1.4(−2)	1.9(−2)	1.60(−2)	4.39(−2)	1.40(−1)	2.16(−1)	2.28(−1)	2.16(−1)	1.01(−1)
$M_3M_5(^3F_3)$		1.93(−2)	2.15(−2)	2.64(−2)	3.98(−2)	5.49(−2)	8.23(−2)	9.80(−2)	1.71(−1)	3.08(−1)
$M_3M_5(^3F_4)$		4.0(−3)	4.0(−3)	6.04(−3)	1.13(−2)	1.56(−2)	2.19(−2)	2.50(−2)	3.71(−2)	5.50(−2)
$M_3M_5(^1D_2)$		1.24(−1)	2.37(−1)	3.33(−1)	3.46(−1)	3.24(−1)	3.08(−1)	3.03(−1)	2.76(−1)	2.41(−1)
$M_4M_4(^1S_0)$										
$M_4M_5(^1G_4)$		3.75	7.01	10.24	11.87	12.32	12.52	12.52	12.07	11.00
$M_5M_5(^3P_0)$		5.0(−4)	5.0(−3)	4.59(−2)	1.23(−1)	1.85(−1)	2.27(−1)	2.37(−1)	2.55(−1)	2.37(−1)
$M_4M_4(^3P_2)$		1.1(−2)	7.3(−2)	1.86(−1)	2.17(−1)	2.19(−1)	2.25(−1)	2.30(−1)	2.36(−1)	2.42(−1)
$M_4M_4(^3P_1)$		1.1(−5)	5.0(−5)	2.32(−4)	6.7(−4)	1.18(−3)	2.02(−3)	2.48(−3)	4.33(−3)	6.85(−3)
$M_4M_5(^1D_2)$		8.9(−2)	1.16(−1)	6.49(−3)	1.46(−2)	4.61(−2)	6.75(−2)	7.32(−2)	8.64(−2)	8.55(−2)
$M_5M_5(^3F_2)$		1.0(−3)	1.9(−2)	1.45(−1)	1.96(−1)	2.08(−1)	2.10(−1)	2.10(−1)	1.98(−1)	1.73(−1)
$M_4M_5(^3F_3)$		2.0(−5)	1.0(−4)	4.88(−4)	1.0(−3)	2.53(−3)	4.51(−3)	5.61(−3)	1.05(−2)	1.94(−2)
$M_5M_5(^3F_4)$		4.0(−3)	3.9(−2)	2.78(−1)	7.15(−1)	1.15	1.52	1.62	1.95	2.05

TABLE V. Theoretical relativistic L_2-MM Auger transition rates (in millatomic units), in intermediate coupling with configuration interaction.

Final state	$_{30}$Zn	$_{36}$Kr	$_{45}$Rh	$_{54}$Xe	$_{60}$Nd	$_{67}$Ho	$_{70}$Yb	$_{80}$Hg	$_{92}$U
$M_1M_1(^1S_0)$	1.57(−1)	1.71(−1)	1.91(−1)	1.98(−1)	2.06(−1)	2.08(−1)	2.10(−1)	2.16(−1)	2.25(−1)
$M_1M_2(^1P_1)$	8.95(−1)	1.20	1.78	2.30	2.53	2.82	2.95	3.45	4.31
$M_1M_2(^3P_0)$	2.58(−1)	3.07(−1)	3.83(−1)	4.66(−1)	5.22(−1)	5.97(−1)	6.33(−1)	7.77(−1)	1.03
$M_1M_3(^3P_1)$	4.01(−1)	3.43(−1)	1.30(−1)	2.02(−2)	1.03(−2)	5.09(−2)	7.00(−2)	1.34(−1)	2.08(−1)
$M_1M_3(^3P_2)$	4.0(−3)	9.0(−3)	2.15(−2)	3.47(−2)	4.43(−2)	5.57(−2)	6.01(−2)	7.50(−2)	9.20(−2)
$M_2M_2(^1S_0)$	1.01	1.52	2.10	2.59	2.92	3.33	3.53	4.31	5.62
$M_2M_3(^1D_2)$	2.54	3.43	4.46	5.25	5.58	5.95	6.09	6.50	6.91
$M_2M_3(^3P_1)$	1.46	1.82	2.31	2.77	3.05	3.39	3.54	4.05	4.74
$M_3M_3(^3P_0)$	2.61(−1)	8.9(−2)	9.9(−4)	1.78(−2)	3.74(−2)	6.18(−2)	7.07(−2)	9.39(−2)	1.02(−1)
$M_3M_3(^3P_2)$	4.61(−1)	3.16(−1)	1.55(−1)	9.74(−2)	1.74(−1)	1.04(−1)	1.17(−1)	1.15(−1)	1.19(−1)
$M_1M_4(^1D_2)$	3.36(−1)	3.50(−1)	4.39(−1)	5.24(−1)	5.80(−1)	6.79(−1)	8.08(−1)	1.17	1.75
$M_1M_4(^3D_1)$	3.6(−2)	4.4(−2)	4.99(−2)	6.0(−2)	6.88(−2)	8.29(−2)	9.08(−2)	1.25(−1)	1.86(−1)
$M_1M_5(^3D_2)$	5.7(−2)	7.8(−2)	7.71(−2)	7.27(−2)	7.08(−2)	1.87(−1)	1.28(−1)	9.76(−2)	9.75(−2)
$M_1M_5(^3D_3)$	8.9(−2)	1.56(−1)	2.43(−1)	2.99(−1)	3.24(−1)	3.40(−1)	3.42(−1)	3.32(−1)	2.94(−1)
$M_2M_5(^1F_3)$	3.63	5.83	7.89	7.95	7.77	7.30	7.13	6.57	5.89
$M_2M_4(^1P_1)$	1.53	2.74	4.02	4.68	4.98	5.20	5.27	5.35	5.20
$M_2M_4(^3D_2)$	1.23	1.86	2.43	3.66(−1)	4.27(−1)	5.61(−1)	6.38(−1)	9.80(−1)	1.63
$M_3M_4(^3D_1)$	3.36(−1)	2.17(−1)	1.89(−1)	4.11(−1)	4.99(−1)	5.09(−1)	5.03(−1)	4.57(−1)	3.77(−1)
$M_2M_5(^3P_2)$	1.20(−1)	2.47(−1)	2.72(−1)	2.72	2.88	2.98	3.01	3.04	2.93
$M_3M_4(^3D_3)$	3.91(−1)	3.12(−1)	1.99(−1)	1.51	2.48	3.36	3.60	3.93	3.76
$M_3M_4(^3P_0)$	9.2(−2)	1.43(−1)	1.99(−1)	2.32(−1)	2.45(−1)	2.51(−1)	2.52(−1)	2.44(−1)	2.22(−1)
$M_3M_5(^3P_1)$	1.46(−1)	2.03(−1)	2.07(−1)	1.43(−1)	1.53(−1)	2.12(−1)	2.33(−1)	2.90(−1)	3.20(−1)
$M_3M_4(^3F_2)$	5.4(−2)	2.6(−2)	1.96(−1)	3.57(−1)	4.15(−1)	4.55(−1)	4.61(−1)	4.46(−1)	3.81(−1)
$M_3M_5(^3F_3)$	1.1(−2)	1.16(−1)	4.89(−1)	4.77(−1)	2.53(−1)	1.59(−1)	1.48(−1)	1.62(−1)	2.01(−1)
$M_3M_5(^3F_4)$	8.9(−4)	9.9(−4)	1.24(−5)	5.5(−4)	1.84(−3)	4.26(−3)	5.55(−3)	1.14(−2)	2.19(−2)
$M_3M_5(^1D_2)$	1.1(−2)	2.6(−2)	3.43(−2)	2.60(−2)	1.40(−2)	8.33(−3)	6.95(−3)	2.99(−3)	1.20(−3)
$M_4M_4(^1S_0)$	2.15(−1)	4.18(−1)	6.89(−1)	8.27(−1)	8.59(−1)	8.58(−1)	8.52(−1)	7.94(−1)	6.83(−1)
$M_4M_5(^1G_4)$	5.46	10.29	15.62	18.77	19.72	20.02	19.92	18.54	15.73
$M_5M_5(^3P_0)$	3.9(−2)	4.7(−2)	9.3(−3)	3.25(−3)	2.56(−2)	4.67(−2)	5.20(−2)	6.51(−2)	5.86(−2)
$M_4M_4(^3P_2)$	2.33(−1)	1.10	3.29	4.56	4.93	5.09	5.11	4.90	4.37
$M_4M_5(^3P_1)$	1.14(−1)	2.07(−1)	3.07(−1)	3.56(−1)	3.71(−1)	3.68(−1)	3.61(−1)	3.22(−1)	2.53(−1)
$M_4M_5(^1D_2)$	9.33(−1)	1.53	1.17	5.86(−1)	4.45(−1)	4.23(−1)	4.19(−1)	4.00(−1)	3.53(−1)
$M_5M_5(^3F_2)$	4.81(−1)	4.51(−1)	1.35(−1)	3.67(−1)	4.67(−1)	5.08(−1)	5.13(−1)	4.98(−1)	4.30(−1)
$M_4M_4(^3F_3)$	7.28(−1)	1.35	1.98	2.35	2.46	2.51	2.50	2.36	2.05
$M_5M_5(^3F_4)$	5.20(−1)	7.25(−1)	4.73(−1)	1.85(−1)	6.45(−2)	5.36(−2)	6.22(−2)	1.28(−1)	1.98(−1)

TABLE VI. Theoretical relativistic L_3-MM Auger transition rates (in milliatomic units), in intermediate coupling with configuration interaction.

Final state	$_{18}$Ar	$_{30}$Zn	$_{36}$Kr	$_{45}$Rh	$_{54}$Xe	$_{60}$Nd	$_{67}$Ho	$_{70}$Yb	$_{80}$Hg	$_{92}$U
$M_1M_1(^1S_0)$	1.35(−1)	1.54(−1)	1.68(−1)	1.87(−1)	1.94(−1)	2.00(−1)	2.00(−1)	1.98(−1)	1.85(−1)	1.41(−1)
$M_1M_2(^1P_1)$	6.65(−1)	7.20(−1)	7.64(−1)	6.43(−1)	3.96(−1)	2.90(−1)	2.12(−1)	1.89(−1)	1.31(−1)	7.68(−2)
$M_1M_2(^3P_0)$	4.0(−6)	3.0(−4)	7.0(−4)	1.32(−3)	2.0(−3)	1.33(−3)	9.83(−4)	7.89(−4)	1.93(−4)	3.32(−4)
$M_1M_3(^3P_1)$	1.18(−1)	1.96(−1)	3.30(−1)	7.21(−1)	1.24	1.51	1.80	1.92	2.31	2.86
$M_1M_3(^3P_2)$	5.51(−1)	6.49(−1)	7.76(−1)	9.74(−1)	1.18	1.32	1.50	1.59	1.91	2.41
$M_2M_2(^1S_0)$	3.78(−1)	3.35(−1)	2.23(−1)	1.05(−1)	5.51(−2)	3.96(−2)	2.66(−2)	2.17(−2)	7.70(−3)	2.14(−4)
$M_2M_3(^1D_2)$	1.70	2.13	2.56	3.04	3.53	3.87	4.32	4.52	5.30	6.56
$M_2M_3(^3P_1)$	5.19(−1)	7.50(−1)	9.43(−1)	1.21	1.47	1.64	1.85	1.95	2.29	2.81
$M_3M_3(^3P_0)$	1.38(−1)	4.07(−1)	7.16(−1)	1.11	1.44	1.62	1.83	1.92	2.23	2.66
$M_3M_3(^3P_2)$	1.47	2.19	2.88	3.79	4.37	3.45	4.73	6.10	7.18	8.13
$M_1M_4(^1D_2)$		3.52(−1)	3.69(−1)	4.37(−1)	6.62(−1)	1.65	4.22(−1)	3.01(−1)	4.09(−1)	7.44(−1)
$M_1M_4(^3D_1)$		3.4(−2)	5.9(−2)	8.76(−2)	1.04(−1)	1.10(−1)	1.12(−1)	1.10(−1)	9.78(−2)	7.52(−2)
$M_1M_5(^3D_2)$		6.3(−2)	1.01(−1)	1.88(−1)	3.40(−1)	8.29(−1)	1.42	4.60(−1)	3.51(−1)	8.27(−1)
$M_1M_5(^3D_3)$		9.1(−2)	1.31(−1)	1.80(−1)	2.30(−1)	2.65(−1)	3.19(−1)	3.50(−1)	4.89(−1)	7.89(−1)
$M_2M_5(^1F_3)$		3.29	4.85	5.54	4.70	4.32	3.80	3.60	3.04	2.46
$M_2M_4(^1P_1)$		8.22(−1)	9.16(−1)	6.63(−1)	4.97(−1)	4.51(−1)	4.19(−1)	4.11(−1)	3.93(−1)	3.98(−1)
$M_2M_4(^3D_2)$		3.11(−1)	4.15(−1)	5.33(−1)	1.62(−1)	1.35(−1)	1.16(−1)	1.08(−1)	8.80(−2)	8.44(−2)
$M_3M_4(^3D_1)$		5.28(−1)	1.21	2.24	2.44	2.15	2.12	2.14	2.25	2.50
$M_3M_4(^3P_2)$		7.37(−1)	6.64(−1)	2.23(−1)	5.90(−1)	6.49(−1)	6.92(−1)	7.10(−1)	7.54(−1)	7.95(−1)
$M_3M_4(^3D_3)$		1.30	2.31	3.97	5.28	5.28	5.53	5.65	5.81	6.13
$M_3M_4(^3P_0)$		1.04(−1)	1.64(−1)	2.38(−1)	3.13(−1)	3.65(−1)	4.33(−1)	4.66(−1)	5.88(−1)	7.79(−1)
$M_3M_5(^3P_1)$		3.89(−1)	6.37(−1)	1.04	1.89	2.72	3.27	3.43	3.86	4.16
$M_3M_4(^3F_2)$		8.7(−2)	6.67(−1)	1.60	1.97	2.08	2.23	2.31	2.54	2.89
$M_2M_5(^3F_3)$		7.5(−2)	2.25(−1)	9.02(−1)	2.55	4.03	5.33	5.73	7.00	8.00
$M_3M_5(^3F_4)$		2.78(−2)	2.73(−2)	1.90(−2)	1.81(−2)	1.68(−2)	1.88(−2)	2.12(−2)	3.31(−2)	6.14(−2)
$M_3M_5(^1D_2)$		1.20(−1)	2.25(−1)	4.17(−1)	6.80(−1)	8.75(−1)	1.05	1.11	1.29	1.45
$M_4M_4(^1S_0)$		2.06(−1)	3.66(−1)	4.59(−1)	4.30(−1)	3.75(−1)	3.47(−1)	3.44(−1)	3.22(−1)	3.14(−1)
$M_4M_5(^1G_4)$		5.64	10.51	15.45	18.43	19.43	20.48	20.96	21.80	22.50
$M_5M_5(^3P_0)$		2.1(−2)	6.3(−2)	2.18(−1)	4.30(−1)	5.88(−1)	7.08(−1)	7.50(−1)	8.63(−1)	9.49(−1)
$M_4M_4(^3P_2)$		2.1(−1)	6.52(−1)	1.10	1.16	1.16	1.21	1.24	1.30	1.35
$M_4M_5(^3P_1)$		6.1(−2)	1.17(−1)	1.89(−1)	2.46(−1)	2.80(−1)	3.13(−1)	3.27(−1)	3.61(−1)	3.83(−1)
$M_4M_5(^1D_2)$		8.4(−1)	1.03	7.42(−1)	1.48	1.97	2.33	2.45	2.77	3.00
$M_5M_5(^3F_2)$		5.25(−1)	1.35	2.89	3.38	3.53	3.75	3.86	4.07	4.26
$M_4M_5(^3F_3)$		6.91(−1)	1.32	2.04	2.58	2.85	3.10	3.21	3.45	3.65
$M_5M_5(^3F_4)$		1.11	2.30	4.33	6.47	8.02	9.44	9.95	11.43	12.59
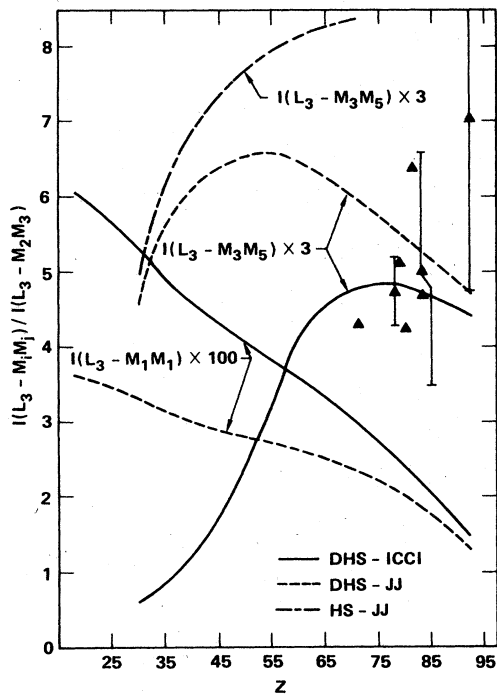
FIG. 2. Ratio of calculated L_3-M_1M_1 and L_3-M_3M_5 Auger rates to L_3-M_2M_3 Auger rates, as functions of atomic number. The solid curves represent Dirac-Hartree-Slater results in intermediate coupling with configuration interaction, the dashed curves indicate the Dirac-Hartree-Slater results in j-j coupling, and the dotted-dashed curve represents the nonrelativistic Hartree-Slater results in j-j coupling, all from the present work. The experimental results are from Ref. 24—32.
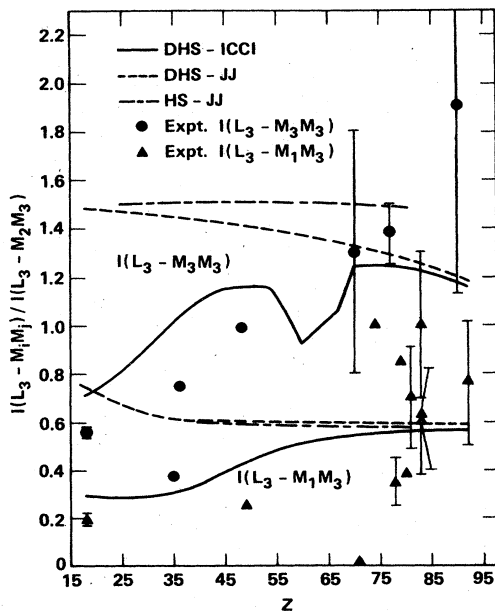
FIG. 3. Ratio of calculated L_3-M_1M_3 and L_3-M_3M_3 Auger rates to L_3-M_2M_3 Auger rate; see caption of Fig. 2 for details. The dip in $I(L_3$-$M_3M_3)/I(L_3$-$M_2M_3)$ ratio near $Z=63$ is caused by level crossing (see text).
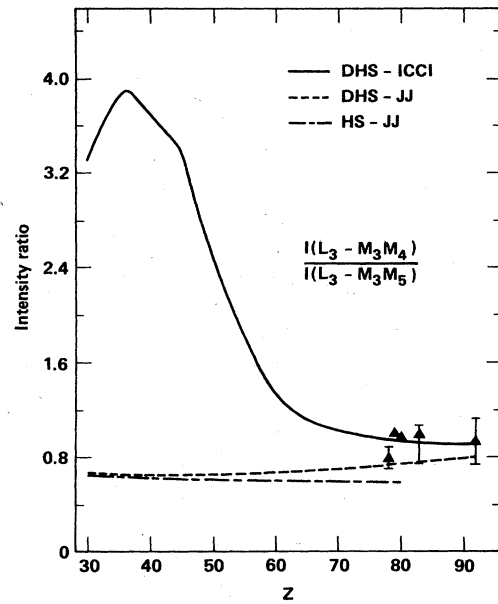
FIG. 4. Ratio of calculated L_3-M_3M_4 Auger rate to L_3-M_3M_5 Auger rate as a function of atomic number. The legend is the same as in Fig. 2.

crease the L_3-M_1M_1 rate by a factor 1.5—2 for $Z \leq 45$. For all the relative intensities studied in the present work, good agreement is found between theory from relativistic intermediate coupling with configuration interaction and experiment, considering the scarcity and uncertainty of experimental data.

For $Z < 60$, the $M_3M_3(J=2)$ level lies above the $M_1M_4(J=2)$ and $M_1M_5(J=2)$ levels. As Z increases, $M_3M_3(J=2)$ first comes down to cross $M_1M_4(J=2)$ at $Z \approx 62$, then crosses $M_1M_5(J=2)$ at $Z \approx 65$.[3] Similar to
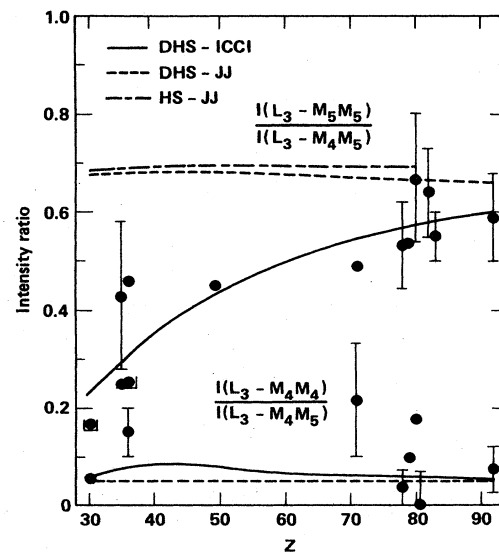
FIG. 5. Ratio of calculated L_3-M_5M_5 Auger rate to L_3-M_4M_5 Auger rate; see caption of Fig. 2 for details.

TABLE VII. Comparison between selected theoretical $L_2\text{-}M_1M_{23}$ and $L_2\text{-}M_{23}M_{45}$ Auger energies (in eV) and transition rates (in a.u.) for $_{36}$Kr.

	Energy		Rate	
Final state	DHS-ICCI	MCDF	DHS-ICCI	MCDF
$M_1M_2(^1P_1)$	1174.6	1174.6	1.20(-3)	1.42(-3)
$M_1M_3(^3P_1)$	1195.5	1195.4	3.43(-4)	4.75(-4)
$M_2M_4(^1P_1)$	1380.6	1380.4	2.74(-3)	3.01(-3)
$M_3M_4(^3D_1)$	1391.4	1391.3	2.17(-4)	2.82(-4)
$M_3M_5(^3P_1)$	1395.3	1395.3	2.03(-4)	2.40(-4)
$M_1M_3(^3P_2)$	1200.2	1200.1	9.0(-6)	1.6(-6)
$M_2M_4(^3D_2)$	1388.4	1388.3	1.86(-3)	2.28(-3)
$M_2M_5(^3P_2)$	1392.9	1392.9	2.47(-4)	3.70(-4)
$M_3M_4(^3F_2)$	1396.9	1396.9	2.6(-5)	2.17(-5)
$M_3M_5(^1D_2)$	1402.3	1402.2	2.6(-5)	2.04(-5)
$M_3M_5(^3F_3)$	1400.9	1400.9	1.16(-4)	4.65(-5)
$M_2M_5(^1F_3)$	1378.6	1378.4	5.83(-3)	6.22(-3)
$M_3M_4(^3D_3)$	1393.4	1393.4	3.12(-4)	4.46(-4)

the $K\text{-}M_1M_{4,5}(J=2)$ and $K\text{-}M_3M_3(J=2)$ transitions,[3] the level-crossing interaction among $M_3M_3(J=2)$, $M_1M_4(J=2)$, and $M_1M_5(J=2)$ levels at the neighborhood of $Z=63$ has a strong influence on these transition rates. The $L_1\text{-}M_3M_3(^3P_2)$ and $L_3\text{-}M_1M_{4,5}(J=2)$ have strong peaks at $Z=63$ (Fig. 6). These weak transitions $L_1\text{-}M_3M_3(^3P_2)$ and $L_3\text{-}M_1M_{45}(J=2)$ pick up their intensities from coupling with strong transitions $L_1\text{-}M_1M_{4,5}(J=2)$ and $L_3\text{-}M_3M_3(J=2)$, respectively. This level-crossing interaction increases the $L_1\text{-}M_3M_3(^3P_2)$ in-

FIG. 6. Calculated $L_1\text{-}M_3M_3(^3P_2)$ and $L_3\text{-}M_1M_{4,5}(J=2)$ Auger rates, as functions of atomic number. The Dirac-Fock-Slater calculations in intermediate coupling with configuration interaction (solid curves) exhibit a pronounced peak near $Z=63$, caused by leveling crossing (see text). The dashed curves represent Dirac-Hartree-Slater results in $j\text{-}j$ coupling.

tensity at $Z=60$ by a factor of 50. The strong dip at $Z=60$ in the relative intensity of $I(L_3\text{-}M_3M_3)/I(L_3\text{-}M_2M_3)$ as a function Z (Fig. 3) is also the result of level-crossing interaction.

In order to assess the reliability of the Dirac-Hartree-Slater calculations with fixed $j\text{-}j$ basis states, we have performed a sample calculation using multiconfiguration Dirac-Fock approach (MCDF) for $L_2\text{-}M_1M_{23}$ and $L_2\text{-}M_{23}M_{45}$ transitions of Kr. In the MCDF calculations, the energies and wave functions for bound states were computed with extended averaged level scheme (EAL).[33] In the EAL scheme, the orbital wave functions are obtained by minimizing the statistically averaged energy of all the levels. We use single configuration for an initial hole state and 16-configuration-state functions expansion from $[3s3p]$ and $[3p3d]$ double-hole configurations for the final Auger states. The Auger energies were obtained by taking the differences between initial- and final-state energies. However, in the calculations of Auger transition rates, the orbital wave functions from an initial state were used to avoid the complication from nonorthogonality between the initial and final orbital wave functions. The continuum wave functions were generated by solving the Dirac-Fock equations corresponding to final hole state without including the exchange interaction between bound and continuum electrons. The continuum wave functions were then Schmidt orthogonalized to the initial orbital wave functions. The results are listed in Table VII. The Auger energies from DHS-ICCI agree within 0.2 eV with the results from the MCDF model. For the Auger rates, the results from these two theories agree within $\sim 25\%$ except for the very weak transitions. Certainly, in order to test the relativistic intermediate coupling theory, more precise experimental data are needed.

ACKNOWLEDGMENTS

[1]M. H. Chen, B. Crasemann, and H. Mark, Phys. Rev. A 21, 442 (1980).

[2]W. N. Asaad and D. Petrini, Proc. R. Soc. London, Ser. A 350, 381 (1976).

[3]M. H. Chen, B. Crasemann, and H. Mark, Phys. Rev. A 27, 1213 (1983).

[4]W. N. Asaad, Nucl. Phys. 66, 494 (1965).

[5]W. Mehlhorn and W. N. Asaad, Z. Phys. 191, 231 (1966).

[6]M. H. Chen and B. Crasemann, Phys. Rev. A 8, 7 (1973).

[7]H. P. Kelly, Phys. Rev. A 11, 556 (1975).

[8]G. Howat, T. Åberg, and O. Goscinski, J. Phys. B 11, 1575 (1978).

[9]S. Aksela and J. Väyrynen, Phys. Rev. Lett. 33, 999 (1974).

[10]W. Mehlhorn and D. Stalherm, Z. Phys. 217, 294 (1968).

[11]D. A. Shirley, Phys. Rev. A 7, 1520 (1973).

[12]F. P. Larkins, At. Data Nucl. Data Tables 20, 311 (1977).

[13]C. Møller, Ann. Phys. (Leipzig) 14, 531 (1932).

[14]K. N. Huang, M. Aoyagi, M. H. Chen, B. Crasemann, and H. Mark, At. Data Nucl. Data Tables 18, 243 (1976).

[15]M. H. Chen, E. Laiman, B. Crasemann, M. Aoyagi, and H. Mark, Phys. Rev. A 19, 2253 (1979).

[16]C. Briancon and J. P. Desclaux, Phys. Rev. A 13, 2157 (1976).

[17]D. R. Beck and C. A. Nicolaides, in Excited States in Quantum Chemistry, edited by C. A. Nicolaides and D. R. Beck (Reidel, Dordrecht, 1978).

[18]M. Ohno and G. Wendin, J. Phys. B 12, 1305 (1979).

[19]U. Fano, Phys. Rev. 124, 1866 (1961).

[20]M. H. Chen, B. Crasemann, and H. Mark, Phys. Rev. A 24, 1158 (1981).

[21]K. Jankowski, P. Malinowski, and M. Polasik, J. Chem. Phys. 76, 1 (1982).

[22]S. Aksela and H. Aksela, Phys. Lett. 48A, 19 (1974).

[23]T. Kondow, T. Kawai, K. Kunimori, T. Onishi, and K. Tamaru, J. Phys. B 6, L156 (1973).

[24]S. K. Haynes, U. S. Atomic Energy Commission Report No. CONF-720404, 1973 (unpublished), Vol. I, p. 559.

[25]L. H. Toburen and R. G. Albridge, Nucl. Phys. A90, 529 (1967).

[26]M. J. Zender, W. Pou, and R. G. Albridge, Z. Phys. 218, 245 (1969).

[27]K. Risch, Z. Phys. 159, 89 (1960).

[28]J. C. Nall, G. L. Baird, and S. K. Haynes, Phys. Rev. 118, 1278 (1960).

[29]Z. Sujkowski and O. Melin, Ark. Fys. 20, 193 (1961).

[30]S. K. Haynes, M. Velinsky, and L. J. Velinsky, Nucl. Phys. A90, 573 (1967).

[31]J. Gizon, A. Gizon, and J. Valentin, Nucl. Phys. A120, 321 (1968).

[32]R. Päschke, Z. Phys. 176, 143 (1963).

[33]I. P. Grant, B. J. McKenzie, P. H. Norrington, D. F. Mayers, and N. C. Pyper, Comput. Phys. Commun. 21, 207 (1980).